Nucleic Acids Research, 2025, **53**, gkae1289
https://doi.org/10.1093/nar/gkae1289
Advance access publication date: 7 January 2025
Gene regulation, Chromatin and Epigenetics

High hydrostatic pressure promotes gene transcription via a cystathionine-β-synthase domain-containing protein in the hyperthermophilic archaeon *Pyrococcus yayanosii*

Cong Li[1,†], Siyuan Li[2,†], Qinghao Song[1], Lin-tai Da[2,*] and Jun Xu[1,*]

[1]State Key Laboratory of Microbial Metabolism, School of Life Sciences and Biotechnology, Shanghai Jiao Tong University, 800 Dongchuan Road, Minhang District, Shanghai, 200240, China
[2]Shanghai Center for Systems Biomedicine, Shanghai Jiao Tong University, 800 Dongchuan Road, Minhang District, Shanghai, 200240, China

[*]To whom correspondence should be addressed. Tel: +86 21 34204051; Email: xujunn@sjtu.edu.cn
Correspondence may also be addressed to Lin-tai Da. Email: darlt@sjtu.edu.cn
[†]The first two authors should be regarded as Joint First Authors.

Abstract

Cystathionine-β-synthase (CBS) domains are ubiquitously prevalent in all kingdoms of life. Remarkably, in archaea, proteins consisting of solely CBS domains are widespread. However, the biological functions of CBS proteins in archaea are still unknown. Here, we identified a high hydrostatic pressure regulator (HhpR) that comprises four CBS domains serving as a transcriptional activator via specifically binding to the UAS (upstream activating sequence) motif situated within the promoter region of an operon in a hyperthermophilic archaeon *Pyrococcus yayanosii* under high hydrostatic pressure (HHP). By combining molecular dynamics simulations, *in vitro* and *in vivo* assays, we revealed the potential binding interfaces between HhpR and its specific DNA binding site. Particularly, one stem–loop region in HhpR (termed as 'Arm') was found to play a critical role in regulating the transcription activity, and the 192 position in the Arm region is an essential site in dictating the conformational changes of HhpR at HHP condition. Our work provides novel insights into the structure–function relationship of CBS-containing proteins that participate in archaeal gene regulation as general transcriptional activators.

Graphical abstract

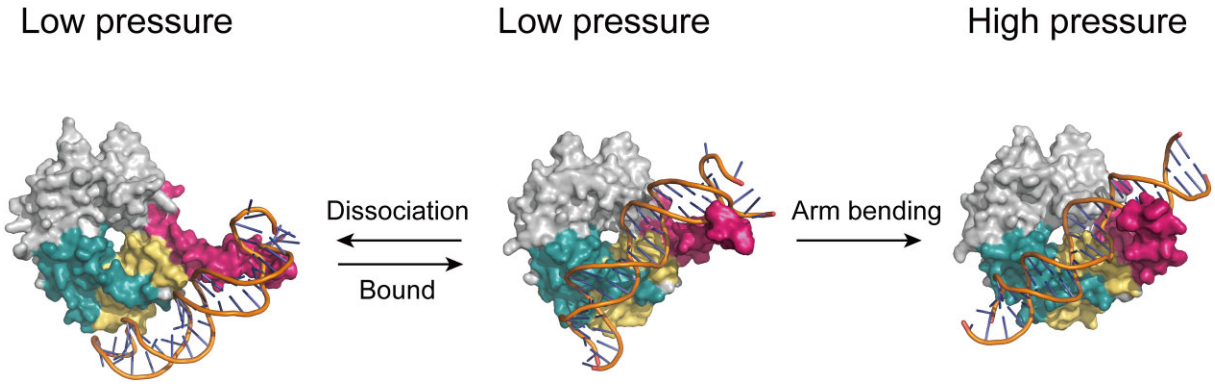

Introduction

The deep sea harbors various types of extreme habitats, which are characterized by high hydrostatic pressure (HHP), high salt concentration, extreme temperatures or pH, and also specialized extracellular electron donors and acceptors in the niches, presenting significant challenges for the inhabiting microorganisms (1). Although HHP is one prevalent environmental factor and considered as the universal key driver of microbial evolution in deep sea (2), our understanding of how microbes adapt to HHP remains limited (3,4). HHP has a significant impact on many physiological activities of microbial cells, and the cell growth under HHP conditions could induce a cascade of stress responses with the concomitant regulation of a series of genes (5,6).

The effects of HHP on microbial physiology are primarily based on studies of a few archaea focusing mainly on the order Thermococcales via omics-based techniques (7,8). Transcriptomic and proteomic analyses of *Pyrococcus yayanosii*, which is the first and only known obligate

Received: June 20, 2024. **Revised:** December 13, 2024. **Editorial Decision:** December 16, 2024. **Accepted:** December 24, 2024

piezophilic hyperthermophilic archaeon (9,10), revealed that several genes involved in translation, chemotaxis and energy metabolism could be regulated by HHP (8). Thus, it can be expected that these pressure-regulated gene expressions might be coordinated by specialized transcription factors (TFs) to promote the adaptability of archaea in harsh environment. To date, several TFs have been identified in Thermococcales, but none of them are linked to HHP (11–15).

Cystathionine-β-synthase (CBS) domain, consisting of ∼60 amino acid residues, commonly presents as tandem repeats in numerous cytosolic and membrane-associated proteins that existed throughout all kingdoms of life (16,17). The CBS domains play both structural and functional roles in biological systems. Previous research has demonstrated that the inosine 5′-monophosphate dehydrogenase of *Escherichia coli* could bind to single-stranded CT-rich DNA and RNA through its CBS domain to inhibit adenylate nucleotide biosynthesis (18,19). Remarkably, in archaea, proteins consisting of solely CBS domains are widespread. Although the nucleic acid binding capacity of the CBS domain protein MJ0729 (tandem repeats of two CBS domains) has been observed in the archaeon *Methanocaldococcus jannaschii* (20), the functional roles of other counterparts of MJ0729, such as MJ1225 (tandem repeats of four CBS domains) from *M. jannaschii* and ST2348 (tandem repeats of two CBS domains) from *Sulfolobus solfataricus* (21,22), are still unknown.

Here, we discovered a pressure-regulated transcriptional activator, HhpR (high hydrostatic pressure regulator), from an archaeon *P. yayanosii*. HhpR, exclusively composed of four tandem copies of CBS domains, could specifically bind to the upstream activating sequence (UAS) of an HHP-inducible promoter P_{hhp}, and the binding affinity of HhpR to P_{hhp} is notably strengthened when subjected to HHP. Further structural modeling and molecular dynamics (MD) simulations indicate that HhpR interacts with P_{hhp} mainly via one loop motif containing K67–D69 and one crucial stem–loop region in HhpR (termed as an Arm region). Computation-based mutagenesis of HhpR reveals that the Arm region plays an essential role in the pressure-regulated properties of HhpR. We further pinpointed one specific residue from the Arm region, S192, that is directly involved in dictating the structural changes of the Arm region at high pressure, as validated by *in vivo* mutagenesis assays. Notably, HhpR-like or CBS-containing proteins are widely distributed in Thermococcales, suggesting that HhpR or similar CBS-containing proteins may play a universal role in regulating the gene expression in hyperthermophilic archaea.

Materials and methods

Strains, plasmids and growth conditions

The strains, plasmids and primers used in the present study are listed in Supplementary Tables S6 and S7. *Escherichia coli* DH5α was employed for performing general DNA manipulation procedures, while *E. coli* Rosetta (DE3) was used for heterologous gene expression purposes. *Escherichia coli* strains were cultured in lysogeny broth (LB) medium at 37°C containing 100 μg/ml ampicillin or 50 μg/ml kanamycin. *Pyrococcus yayanosii* A1 was cultured under anaerobic conditions in Thermococcales rich medium (TRM) at 95°C (23). TRM contains (per liter distilled water) 4 g tryptone, 1 g yeast extract, 3.3 g PIPES disodium salt, 23 g NaCl, 5 g $MgCl_2{\cdot}6H_2O$, 0.7 g KCl, 0.5 g $(NH_4)_2SO_4$, 1 ml of 5% KH_2PO_4, 1 ml of 5% K_2HPO_4, 1 ml of 2% $CaCl_2{\cdot}2H_2O$, 0.05 g NaBr, 0.01 g $SrCl_2{\cdot}6H_2O$, 1 ml of 10 mM Na_2WO_4, 1 ml of 25 mM $FeCl_3$ and 1 mg resazurin. The medium was adjusted to pH 6.8 before autoclave and then reduced with 0.5 g sodium sulfide before use. *Thermococcus eurythermalis* A101 (a subspecies of *T. eurythermalis* A501, without plasmid) and *Thermococcus kodakarensis* TS559 (an agmatine, tryptophan and guanine auxotrophic strain of *T. kodakarensis* KOD1) were cultured in a nutrient-rich medium ASW-YT-S^0 under strictly anaerobic conditions at 85°C (24). The ASW-YT medium contains (per liter distilled water) 20 g NaCl, 3 g $MgCl_2{\cdot}6H_2O$, 6 g $MgSO_4{\cdot}7H_2O$, 1 g $(NH_4)_2SO_4$, 200 mg $NaHCO_3$, 300 mg $CaCl_2{\cdot}2H_2O$, 0.5 g KCl, 420 mg KH_2PO_4, 50 mg NaBr, 20 mg $SrCl_2{\cdot}6H_2O$ and 10 mg $(NH_4)_2Fe(SO_4)_2{\cdot}6H_2O$; 0.5% (w/v) yeast extract; and 0.5% (w/v) tryptone supplemented with 1× trace mineral solution (1 l of 1000× contains 0.5 g $MnSO_4{\cdot}H_2O$, 0.1 g $CoCl_2{\cdot}6H_2O$, 0.1 g $ZnSO_4{\cdot}7H_2O$, 0.01 g $CuSO_4{\cdot}5H_2O$, 0.01 g $AlK(SO_4)_2{\cdot}12H_2O$, 0.01 g H_3BO_3, 0.01 g $Na_2MoO_4{\cdot}2H_2O$) and 1× vitamin mixture (1 l of 200× contains 0.2 g niacin, 0.08 g biotin, 0.2 g pantothenate, 0.2 g lipoic acid, 0.08 g folic acid, 0.2 g *p*-aminobenzoic acid, 0.2 g thiamine, 0.2 g riboflavin, 0.2 g pyridoxine and 0.2 g cobalamin). The ASW-YT-S^0 medium was the ASW-YT medium supplemented with 0.2% (w/v) sulfur. Transformants of *P. yayanosii* A1 and other Thermococcales were selected at a final concentration of 10 and 4 μM of simvastatin (Sim), respectively (25). Agmatine (1 mM) was added during the cultivation of *T. kodakarensis* TS559. The solid media were generated by adding 1.5% (w/v) Gelrite® as described previously (25). DNA concentration of the plasmids was determined by NanoPhotometer™ N50 (Implen, Germany).

Truncation mutation of TK1626

To eliminate the influence of the native homologue of HhpR, a truncation mutation was attempted on the encoding gene for TK1626 in *T. kodakarensis* (Supplementary Figure S9). By employing whole-plasmid polymerase chain reaction (PCR), a set of mutated *hhpR* gene fragments were integrated into the pTE vector, respectively. The resulting plasmids were then introduced into the *T. kodakarensis* TS559 strain and selected on rolling tubes without the addition of agmatine.

A suicide plasmid, pUS1626s, was constructed for the purpose of creating a truncated version of the TK1626 coding gene. The plasmid pUC18 was fused with the upstream fragment TK1626-up (1500 bp), a Sim^R cassette and a fragment harboring the engineered target gene TK1626 (1500 bp) carrying a nonsense mutation at codon 3 for the generation of pUS1626s.

Subsequently, pUS1626s was introduced into the *T. kodakarensis* TS559 transformant strains carrying the mutated *hhpR* gene and subjected to selection with 4 μM simvastatin, to generate TK1626 truncation mutant strains.

Protein expression and purification

For purification of CBS domain-containing protein HhpR and its homologous protein TK1626, N-terminal 6×His-tag fusions were constructed. DNA fragments that encode proteins HhpR and TK1626 were amplified by PCR from

genomic DNA and fused into pET-28a using ClonExpress II One-Step Cloning Kit (Vazyme). Plasmids encoding mutant HhpR proteins were prepared by whole-plasmid PCR mutagenesis. Expression plasmids for truncated versions of HhpR were constructed into the pET-22a by cloning DNA fragments encoding one, two or three tandem repeated CBS domains. The recombinant plasmids were transformed into *E. coli* Rosetta (DE3).

Cultures of *E. coli* were grown in LB medium at 37°C to $A_{600} \sim 0.6$, then induced with 0.1 mM isopropyl β-D-1-thiogalactopyranoside and shifted to 20°C for 16 h. The cells were harvested by centrifugation at 10 000 × *g* at 4°C for 5 min using Centrifuge 5425 R (Eppendorf, Hamburg, Germany) and resuspended in a lysis buffer containing 50 mM Tris (pH 8.0) and 500 mM NaCl. Proteins were purified by Ni NTA Beads 6FF (Smart-Lifesciences). The proteins bound to the column were eluted using a linear gradient of imidazole ranging from 20 to 500 mM in concentration. The obtained HhpR protein was further purified by gel filtration chromatography using a Superdex 200 Increase 10/300 GL column (Cytiva) in 20 mM Tris (pH 8.0) and 300 mM NaCl. The purified proteins were analyzed on 12% sodium dodecyl sulfate–polyacrylamide gel electrophoresis (SDS–PAGE), and all protein concentrations were quantified using a Bradford assay (Sangon, Shanghai, China).

Screen for HHP-tolerant β-glucosidase from deep-sea thermophilic archaea

To quantify the strength of the promoter under HHP condition, we screened and characterized three β-glycosidases, encoded by *TERMP_00966*, *TEU_03570* and *BD01_1339*, from *Thermococcus barophilus* MP, *T. eurythermalis* A501 and *T. nautili* 30-1, respectively. The β-glycosidase-encoding gene fragment was cloned into the pTE1 plasmid under the control of a constitutive promoter P_{gdh}. Overlap sequences of 15 bp, corresponding to the linearized plasmid ends, were integrated into the primer sequences for the amplification of the targeted protein coding sequence. The PCR product was ligated to the linearized pTE1 using ClonExpress II One-Step Cloning Kit, resulting in three plasmids named pTEgalTEU_0357, pTEgalBD01_1339 and pTEgluTERMP_00966. The recombinant plasmid was purified using Omega Kit and then transformed into *T. kodakarensis* TS559 (23). Transformant cells of *T. kodakarensis* TS559 were cultured at 85°C for 12 h. The cells were harvested by centrifugation at 10 000 × *g* at 4°C for 5 min using Centrifuge 5425 R (Eppendorf, Hamburg, Germany) and resuspended in a lysis buffer containing 50 mM Tris (pH 8.0) and 500 mM NaCl. The clarified lysate was loaded onto 1 ml Ni NTA Beads equilibrated with lysis buffer. Proteins were eluted with lysis buffer of a linear 20–250 mM imidazole gradient. The purified proteins were individually transferred into sterilized syringes and incubated under various hydrostatic pressures (0.1, 10, 30 and 50 MPa) at 85°C for 2 h. The syringes were placed in high-pressure vessels (Feiyu Science and Technology Exploitation Co., Ltd, Nantong, China), and the hydrostatic pressure was applied with a water pump (Top Industrie, France). The activity of β-glucosidase and β-galactosidase was evaluated at 85°C.

β-Glucosidase reporter assays

β-Glycosidase activity was measured using *ortho*-nitrophenyl-β-D-glucopyranoside (ONP-gluco) as a substrate with an absorption at 405 nm as described elsewhere (26). Briefly, the culture was adjusted to a standardized cell density after overnight incubation and subsequently resuspended in the lysis buffer. β-glycosidase was assessed following incubation at 85°C in 50 mM sodium phosphate buffer (pH 6.5) supplemented with 2.8 mM ONP-glucoside.

Affinity purification of the putative transcription factor

Dynabeads™ M-280 Streptavidin (Invitrogen, 11205D) was used to capture proteins. The detailed method is based on Thermo Fisher Scientific publication (No. MAN0014017, https://qa1.thermofisher.cn/order/catalog/product/cn/en/11205D). Biotin-labeled (Sangon, Shanghai, China) heat shock promoter (P_{hsp}) sequences (amplified using primer pair P_{hsp}-bio-F/P_{hsp}-bio-R) and unlabeled P_{hbp} sequences (amplified using primer pair P_{hbp}-F/P_{hbp}-R) were used as control to exclude nonspecific binding proteins. *Pyrococcus yayanosii* A1 cultivated in TRM medium were harvested by centrifugation at 8000 × *g* for 15 min at 4°C and sonicated on ice. Cytoplasmic proteins of *P. yayanosii* A1 were harvested by centrifugation at 13 000 × *g* for 30 min at 4°C. Released immobilized proteins were separated by SDS–PAGE and observed using Pierce Silver Stain Kit (Thermo Fisher Scientific). Band of interest was excised from the polyacrylamide gel and the recovered protein was identified by UPLC–MS/MS analysis (Huada Gene Research Center).

Electrophoretic mobility shift assay

For electromobility shift DNA-binding assays (EMSAs), the *P. yayanosii* A1 HHP operon promoter region was amplified via PCR with one primer 5-labeled with Cy5, followed by a Gel Extraction Kit (Omega, D2500-02). FAM-labeled single-stranded DNA probes were synthesized by Sangon Biotech (Shanghai, China). The appropriate concentration of DNA was mixed with different concentrations of purified protein for 20 min at room temperature (RT). The EMSA reaction buffer (20 μl) contained 40 mM KCl, 12.5 mM Tris (pH 7.5), 1.25 mM $MgCl_2$, 5% (vol/vol) glycerol, 0.5 mM DTT and 0.5 μl of 1 μg/μl poly-d[I-C]. wtHhpR or its mutated variants were incubated at 85°C for 2 h under 0.1 or 52 MPa and then transferred to 0.1 MPa for the EMSA experiments. The mixtures were loaded on 6% nondenaturing polyacrylamide gels at 100 V for 1 h with 0.5× Tris–borate–EDTA buffer under 0.1 MPa at RT. The gels with Cy5-labeled DNA probes were scanned using an Amersham Typhoon RGB Biomolecular Imager (GE, USA). The gels with FAM-labeled DNA probes were detected by ChemiScope 3300 (Clinx Science Instruments, Shanghai, China). EMSA results were consistent findings across three replicates.

DNase I footprinting assay

DNase I footprinting assay was performed as previously described (27). The DNA probe was PCR amplified with a 5′FAM-labeled primer and purified with a Gel Extraction Kit. The reaction system was the same as the EMSA method. After incubation for 20 min at RT, 0.02 U of DNase I was added to the mixture for 10 min at RT. The reaction was stopped by 0.25 μl of 0.5 M EDTA and incubated at 75°C for 15 min.

The digested samples were purified and mixed with GeneScan LIZ500 size standards and analyzed with an Applied Biosystems 3730XL DNA analyzer (identified by Sangon Biotech).

Fluorescence polarization assay

A fluorescence polarization (FP) assay was conducted to determine the affinity of HhpR for double-stranded DNA (dsDNA). A 44-bp dsDNA was produced by incubating a FAM-labeled oligonucleotide (5′-CATATAAAAATTGTTGGGCA AATCTGCCCAGAAAAGCTTAAAAG-3′) and its unlabeled complementary counterpart at 95°C for 10 min, followed by gradual cooling to RT. For the HhpR–dsDNA interaction assay, binding reactions such as EMSA (30 μl) were prepared. dsDNA (50 nM) was incubated with 2-fold serially diluted HhpR protein (0.156–40 μM). HhpR was incubated at 85°C for 2 h under 0.1 or 52 MPa and then transferred to 0.1 MPa for the FP experiments. After a 10-min incubation at RT, FP measurements were taken with a Spark multifunctional microplate reader (Tecan). Binding data were subsequently analyzed with a single-site binding model using GraphPad Prism v.9.5.1.

Structural modeling

We performed molecule docking to construct the HhpR–DNA complex. The structure of HhpR (UniProt: F8AFU3) was predicted using AlphaFold v2.3.1 (28). One 25-bp B-form DNA structure was generated by w3DNA (29), with a sequence of 5′-CGTGCGACATATAAAAATTGTTGGG-3′ that contains a specific binding site for HhpR (Figure 3A). We then employed the HDOCKlite v1.1 stand-alone package to dock HhpR with the modeled DNA (30). Since the EMSAs have confirmed that CBS1-2 can also bind to DNA, we thus conducted molecular docking for both full-length HhpR and CBS1-2 with DNA. The docking structure with the best score was used as the final binding complex, which was then subject to energy minimization using the GROMACS 2022.3 package to relieve the steric clashes. Finally, the minimized structure of the complex was used for the subsequent MD simulations.

Setup of MD simulation

All the MD simulations were performed using the GROMACS 2022.2 package (31), The HhpR–DNA complex was centered in a dodecahedron box with a minimal system and box wall distance set to 10.0 Å. The whole system was solvated in a TIP4P/2005 water box that is one of the most reliable water models for studying pressure effects (32). Predictions of the isothermal compressibility of water at 298 K by the TIP4P/2005 model are in excellent agreement with experiment in the pressure range 0.1–100 MPa (33). To neutralize the system and ensure an ionic concentration of 0.3 M, we added 216 Na^+ and 169 Cl^- ions. The final system contains 121 469 atoms. The protein/DNA were described using the AMBER force field ff14SB, with the bsc1 corrections used for the DNA nucleotides (34,35). The complex was simulated at three different pressures of 0.1, 20 and 52 MPa. Under each pressure condition, we first performed energy minimization using the steepest-descent algorithm. Then, one 200-ps NVT equilibration was performed at 358 K, followed by 200-ps NPT equilibrium MD simulations by constraining all of the solute heavy atoms. Finally, three parallel 200-ns production MD simulations were conducted under each pressure, initiated at varied velocities; the last 150 ns are used for all subsequent analysis. We adopted the V-Rescale thermostat to maintain the temperature at 358 K and the Parrinello–Rahman barostat to maintain the pressure. Because the compressibility of water changes drastically with pressure, we used different compressibility values for water, namely 4.5×10^{-5} bar^{-1} at 0.1 MPa, 4.3×10^{-5} bar^{-1} at 20 MPa and 3.98×10^{-5} bar^{-1} at 52 MPa, according to a previous study (36). Particle mesh Ewald was used for long-range electrostatics, and a cutoff of 12 Å was used for short-range electrostatics and van der Waals interactions. Analyses of the DNA conformations, e.g. the bending angle, groove width, etc., were performed using the Curves+ v3.0 software from Bioconda (37).

Phylogenetic analysis

To investigate the evolutionary relationships of HhpR proteins, a phylogenetic tree was constructed based on protein sequences. Initially, the protein sequence of HhpR was used as a query in BLAST to retrieve homologous sequences, collecting the top 50 sequences with high similarity. Sequences lacking comprehensive taxonomic information were excluded from further analysis. Additionally, a methanogenic archaeal protein sequence with four CBS domains was selected as the outgroup to root the tree. Multiple sequence alignment of the collected sequences was performed using MUSCLE without further trimming or filtering steps. Phylogenetic inference was conducted using the maximum likelihood method, implemented with the LG + G substitution model, which was selected based on the optimal Bayesian information criterion score. Bootstrap analysis was conducted with 1000 replicates to assess the robustness of clades. All evolutionary analyses were conducted using the MEGA-X package, and the evolutionary tree was visualized using iTOL.

Searching for the UAS motif situated within the promoter regions in Thermococcales

We used FIMO (version 5.5.7) and blastn to search for the UAS motifs situated within the promoter regions of coding genes across the genomes of five strains in the order Thermococcales, including *P. yayanosii* A1, *T. eurythermalis* A501, *Palaeococcus pacificus* DY20341, *Pyrococcus furiosus* DSM 3638 and *T. kodakarensis* KOD1. Each identified UAS motif was further verified to ensure that its location lies in the region upstream of the corresponding coding gene.

Results

Identification of a novel archaeal transcriptional activator responding to high hydrostatic pressure

Our former study found that an HHP-inducible promoter P_{hbp} controls the transcription of the most significantly upregulated gene cluster in *P. yayanosii* A1 cultivated under 52 MPa (25). To evaluate the potency of P_{hbp} across diverse HHP conditions, we selected the genes encoding putative HHP-tolerant β-glycosidases from three *Thermococcus* species isolated from deep-sea environments, including *T. barophilus* MP, *T. eurythermalis* A501 and *T. nautili* 30-1 (Supplementary Table S1). These β-glycosidases were heterologously expressed in *T. kodakarensis* TS559, respectively (Supplementary Figure S1A). All of the three purified proteins displayed β-glycosidase activity under HHP. Since the β-glucosidase of *T. barophilus* MP demonstrated the highest activity, it was selected as the reporter gene for subsequent

studies (Supplementary Figure S1B). We then evaluated the promoter strength of P_{hhp} from *P. yayanosii* A1 under different HHP conditions by quantifying the β-glucosidase activity. Notably, the β-glucosidase activity exhibited a linear increase with the elevation of hydrostatic pressure from 0.1 to 50 MPa, thus confirming the pressure-induced characteristic of P_{hhp} (Figure 1A and Supplementary Table S2). We identified that 29 strains among the entire Thermococcaceae family harbor a similar promoter sequence situated upstream of a putative HHP-inducible operon (Supplementary Figure S2). Multiple sequence alignment of ∼60 bp in the promoters revealed a highly conserved UAS containing 'CATATAAA' that facilitates the interaction between the TFs bound to the promoter and a conserved palindrome sequence upstream of the TATA-box region (Figure 1D and Supplementary Figure S2).

We further examined the activity of β-glucosidase under HHP condition in two closely related stains of *P. yayanosii*, namely *T. eurythermalis* A101 and *T. kodakarensis* KOD1, using the above β-glycosidase reporter system. We found that the expression level of β-glucosidase in *T. eurythermalis* A101 controlled by P_{hhp} is linearly correlated with pressure, whereas this regulation is absent in *T. kodakarensis* KOD1 (Figure 1B and C). We also searched for the UAS motif situated within the promoter regions of the coding genes in five genomes across Thermococcales (Supplementary Table S3). The results indicate that, apart from the promoter P_{hhp}, multiple UAS motifs were identified in each of the five strains, including 3 motifs in *P. yayanosii* A1, 6 motifs in *T. eurythermalis* A501, 16 motifs in *P. pacificus* DY20341, 18 motifs in *P. furiosus* DSM 3638 and 4 motifs in *T. kodakarensis* KOD1. Considering the varied responses to pressure in varied Thermococcaceae strains, we proposed that a potential transcriptional regulator is involved in modulating the gene expression to cope with HHP stress.

We then utilized streptavidin-coupled superparamagnetic beads (Dynabeads M-280, Invitrogen) to capture the proteins interacting with the biotinylated DNA fragments of P_{hhp}. Pull-down experiments were conducted using cytoplasmic proteins extracted from *P. yayanosii* A1 cells cultured under 0.1 and 52 MPa. Intriguingly, one distinct protein band, ∼31 kDa in size, appeared at the 52 MPa condition but not at 0.1 MPa. The following LC–MS/MS analyses (Supplementary Table S4) revealed that the potential P_{hhp} binder is encoded by the gene PYCH_01 350 (WP_013 904 902), termed as HhpR hereafter.

HhpR is exclusively comprised of four CBS domains, as structurally predicted by AlphaFold (Figure 1E). Using an EMSA, we confirmed that HhpR could specifically bind to P_{hhp} at 0.1 MPa (Supplementary Figure S3A). Through DNase I footprinting at 0.1 MPa, two potential binding sites of HhpR were identified in P_{hhp}: 'CTTAAAAG' within the TATA-box region and 'CATATAAAA' within the UAS region (Supplementary Figure S3B). We further treated HhpR at 52 MPa, and then tested its binding to P_{hhp} at 0.1 MPa by EMSA. The results show that the binding affinity of HhpR to P_{hhp} could be substantially increased after HHP treatment (Figure 1G). However, the conformation of the protein under high pressure and low pressure is reversible. Transitioning from 52 to 0.1 MPa results in the HhpR reassuming its atmospheric pressure conformation. To confirm this, HhpR was left at RT under 0.1 MPa for 0, 1 and 2 h after treating under 52 MPa and, at each time point, tested for binding affinity (Figure 1G). The EMSA results show that following the transfer of HhpR from 52 to 0.1 MPa, as the duration of exposure at 0.1 MPa increases, the binding affinity of HhpR gradually returns to the level observed at 0.1 MPa. The FP results performed at 0.1 MPa revealed that the K_d (0.65 μM) following 52 MPa treatment was three times higher than that (1.94 μM) under 0.1 MPa conditions between HhpR and a 44-bp P_{hhp} containing the UAS site and TATA-box (Figure 1F). The FP values of HhpR treated under high pressure were observed higher than those of the untreated (low-pressure) samples at elevated protein concentrations. This result indicates that high pressure may promote protein aggregation, particularly at high protein concentrations. So, we cannot exclude the possibility that the enhanced binding affinity of the protein to the promoter may partially contribute to the observed increase in FP values under these concentrations. We thus concluded that HhpR serves as a transcriptional activator to regulate the expression of HHP-induced genes by recognition of the UAS and TATA-box sites in P_{hhp}.

Deciphering of the interaction interface between promoter P_{hhp} and activator HhpR

To identify the binding interface between HhpR and P_{hhp}, we designed several DNA probes with truncated or site-mutagenic versions of P_{hhp} and conducted EMSA experiments at 0.1 MPa (Figure 2A, P_{hhp}-I-III and M1-3). The results demonstrated a slight reduction in the binding between HhpR and P_{hhp}-I, where the TATA-box was removed. Deletions of both TATA-box and the palindrome sequence could lead to a further weakened binding between HhpR and P_{hhp} (P_{hhp}-II in Figure 2A and B). Notably, removal of the UAS site could abolish the binding of HhpR to P_{hhp}-III, and this adverse effect could not be reversed even with an increased amount of HhpR. This finding strongly suggests that the UAS region is an essential binding site of HhpR. Furthermore, we altered the UAS region to pure-A, pure-T or GC-rich sequences (M1, M2 and M3, respectively; see Figure 2A). The EMSA analysis demonstrated that the binding affinities of HhpR to M1 and M2 remained unchanged, whereas the HhpR binding to GC-rich M3 was profoundly reduced, suggesting that HhpR specifically recognizes the TA-rich sequence in UAS (Figure 2B).

Subsequently, we pinpointed the essential CBS domains that mediate the binding between the HhpR and P_{hhp} by selectively removing one or more CBS domains. These included CBS1, CBS2, CBS1-2 (combination of CBS1 and CBS2) and CBS1-3 (combination of CBS1, CBS2 and CBS3). The EMSA results indicated that neither CBS1 nor CBS2 could bind to P_{hhp} (Figure 2C). However, the combined form CBS1-2 demonstrated pronounced binding with P_{hhp}. Intriguingly, compared to CBS1-2, CBS1-3 exhibited weaker binding affinity to P_{hhp}, suggesting that the inclusion of CBS3 disfavors the substrate recognition. Experimental assays show that truncation of CBS4 could significantly decrease the binding of HhpR to DNA (Figure 2C), suggesting that CBS4 is critical for maintaining the structural stability of HhpR. Taken together, our results suggest that CBS1 and CBS2 are directly involved in DNA recognition, and the presence of CBS3-4 could slightly increase the binding affinity (Figure 2C).

The molecular mechanism of the HhpR activation under high hydrostatic pressure

Based on the above experimental observations, we endeavored to construct an atomic model of the HhpR–DNA

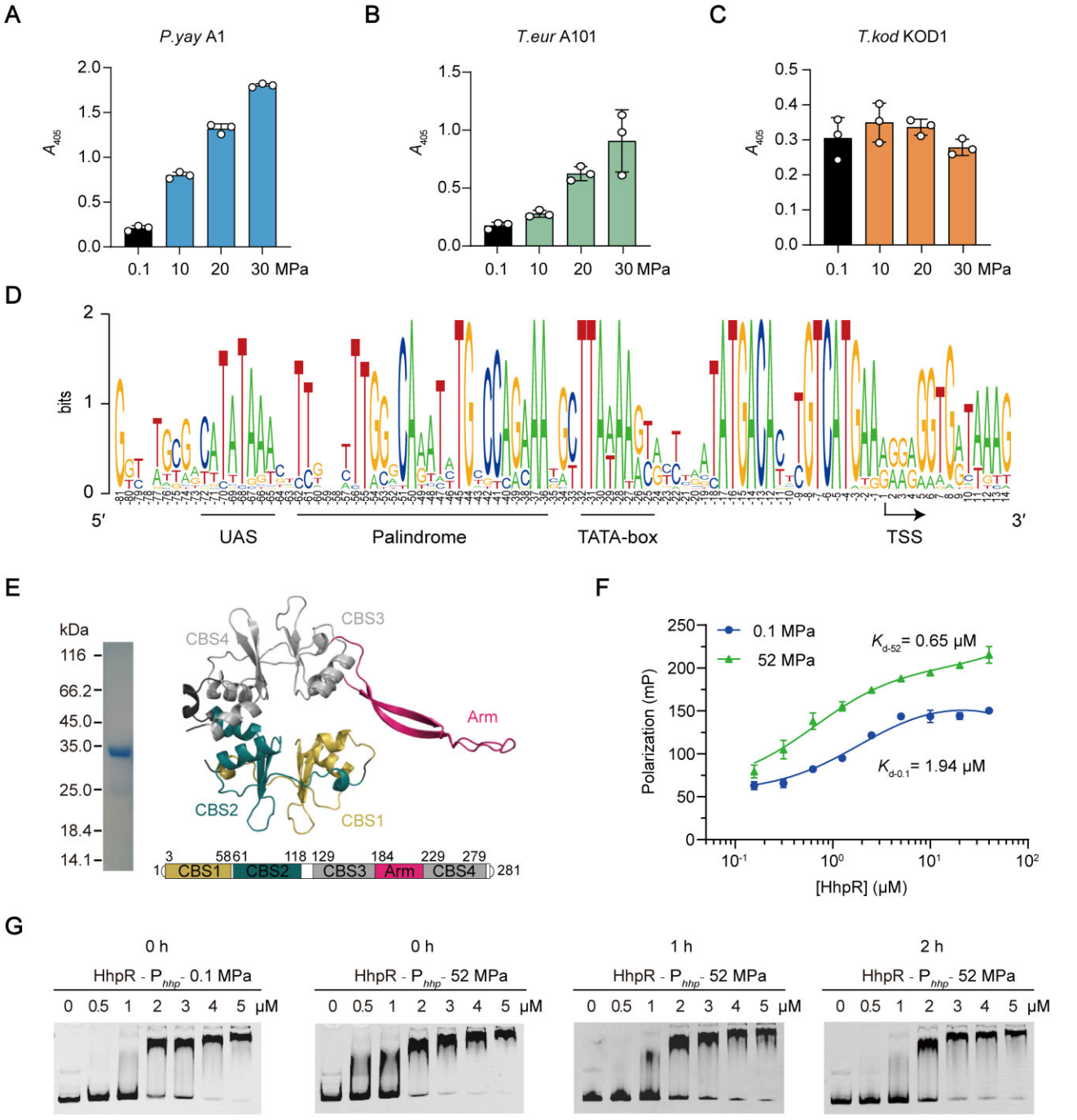

Figure 1. Characterization of the HHP-inducible promoter and identification of the transcriptional activator HhpR. Quantification of the strength of promoter P_{hhp} in strains *P. yayanosii* A1 (**A**), *T. eurythermalis* A101 (**B**) and *T. kodakarensis* KOD1 (**C**) using a piezotolerant β-glucosidase reporter system under under 0.1,10, 20 and 30 MPa. The results are from three independent experiments, and the error bars represent the standard deviations. (**D**) Conservation of the promoter elements of the HHP-inducible promoter in Thermococcales. The promoter elements characterized in the *P. yayanosii* are marked with bars underneath the sequence logo. UAS, upstream activating sequence; Palindrome, imperfect palindrome sequence; TATA-box, TATA-box element. The transcription start site (TSS) is located at the guanine. Promoter sequences of 29 strains of Thermococcales were retrieved from the GenBank public databases using HHP-inducible promoters P_{hhp} of *P. yayanosii* as probes. (**E**) Coomassie Brilliant Blue-stained 12% SDS–PAGE gel evaluation of protein purity for 6×His-tagged HhpR. AlphaFold2 models and structural diagram of the protein HhpR, with each of the four CBS domains highlighted in distinct colors for clarity. (**F**) FP assays showing binding of HhpR to probe 44-bp P_{hhp} at 0.1 MPa ($K_{d\text{-}0.1} = 1.9 \pm 0.40$ μM) and 52 MPa treatment ($K_{d\text{-}52} = 0.65 \pm 0.37$ μM). HhpR was incubated at 85°C for 2 h under 0.1 or 52 MPa. FP experiments were tested under 0.1MPa. Error bars represent the standard deviations calculated from three independent experiments. Binding data were analyzed with a single-site binding model using GraphPad Prism v.9.5.1. (**G**) Analysis of the effect of 0.1 and 52 MPa on the binding of HhpR to promoter P_{hhp} by EMSA and the influence of transferring HhpR from 52 to 0.1 MPa on its binding to the P_{hhp} was examined over time. Protein concentrations in lanes 1–7 were 0, 0.5, 1, 2, 3, 4 and 5 μM, respectively. After treatment at 52 MPa, HhpR was transferred to 0.1 MPa and left at RT for 1 and 2 h. EMSAs were performed at 0.1 MPa.

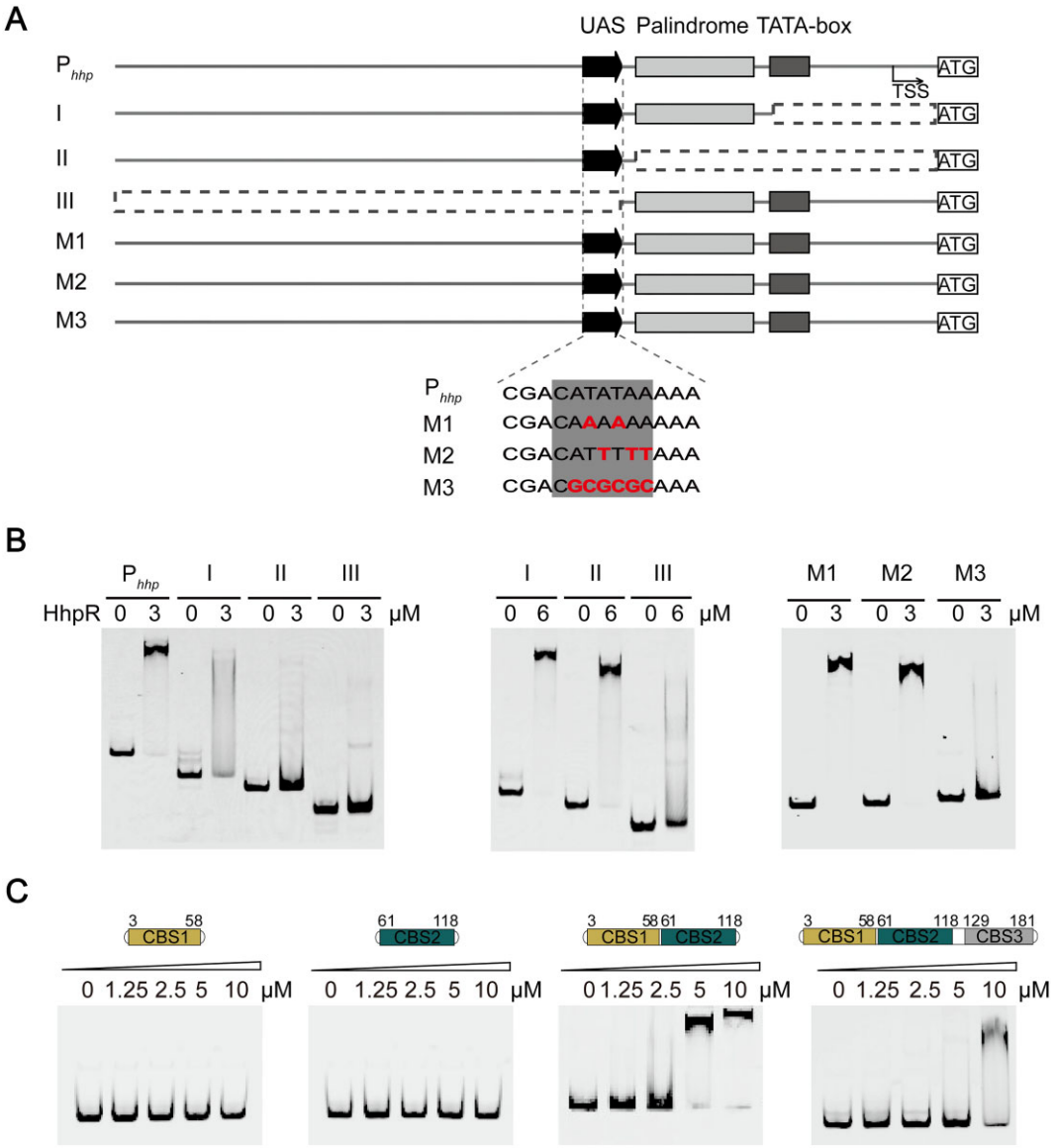

Figure 2. Core regions for the intermolecular binding of P_{hhp} and HhpR. (**A**) Schematic diagram of each truncated DNA fragment or mutation within the UAS site of the promoter P_{hhp}. UAS sequences are represented by a black solid arrow. The TATA-box and putative palindrome are shown as dark and gray boxes, respectively. (**B**) Results of EMSA using fragments I to III as probes with 3 or 6 μM purified HhpR (under 0.1 MPa) and results of EMSA using fragments M1 to M3 as probes with 3 μM purified HhpR (under 0.1 MPa). (**C**) Contributions of the different lengths of truncated HhpR (under 0.1 MPa) to P_{hhp} with EMSA. The rightmost lane contains 10 μM HhpR, and lanes 2–4 contain progressive 2-fold dilutions.

complex using molecular docking strategies. We docked the predicted structure of HhpR to a P_{hhp} sequence (5′-CGTGCGACATATAAAAATTGTTGGG-3′) containing one UAS site, using the HDock method (30). According to the docking score and our experimental observations, we obtained a putative binding mode of the HhpR–DNA complex in which CBS1 and CBS2 reside right at the HhpR–DNA interface, while CBS3 and CBS4 have no direct contact with DNA (Figure 3A). Notably, the AlphaFold structure of HhpR reveals one stem–loop structure (residues 184–229, termed as the Arm region hereafter) connecting CBS3 and CBS4, which is expected to be highly flexible during the DNA recognition.

Thus, to further investigate the structural dynamics of the HhpR–DNA complex, we performed MD simulations for the constructed HhpR–DNA complex at three different pressure conditions (0.1, 20 and 52 MPa). At each condition, we collected 4500 MD snapshots sampled from three parallel 200-ns MD simulations and then projected these MD conformations onto two reaction coordinates: R_g and RMSD of the C_α atoms of HhpR and the P atoms of DNA. The results clearly showt that at 0.1 MPa, two major energy basins could be observed, corresponding to an unbound and a bound state, respectively (Figure 3B). In the unbound state, HhpR tends to dissociate with DNA, reflected from large R_g (∼29 Å) and RMSD (∼12 Å) values (Figure 3E), while in the bound state, a stable HhpR–DNA complex is formed, with R_g and RMSD values of 25.5 and 5 Å, respectively (Figure 3F). In comparison, increasing the pressure to 20 MPa will stabilize the HhpR–DNA structure in a bound state (Figure 3C). This bound state contains two distinguished metastable states, one is a completely bound state and another is a partially bound state, with respective RMSD values

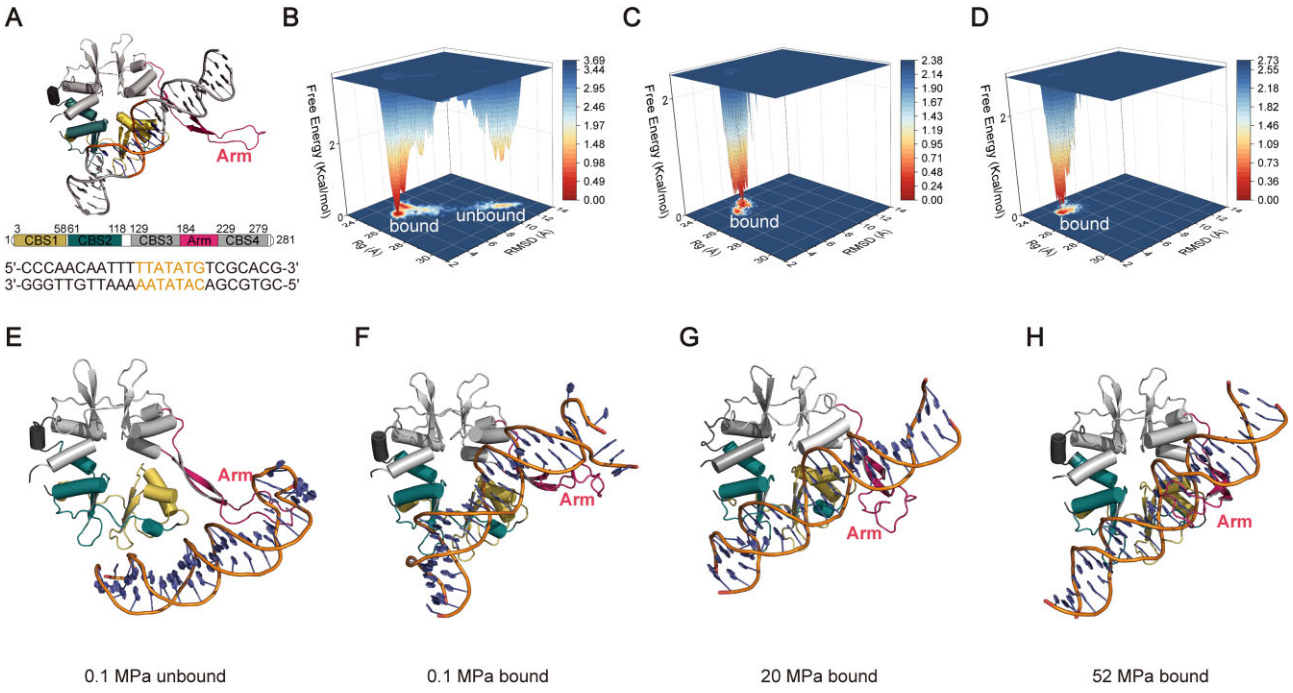

Figure 3. Representative structures of HhpR–DNA complexes under different pressures. (**A**) Docking structure of the HhpR–DNA complex, the DNA core region and the rest of the region were highlighted with different colors for clarity. The complete DNA sequence is shown below the structure. Free energy landscape of HhpR–DNA complexes at 0.1 MPa (**B**), 20 MPa (**C**) and 52 MPa (**D**); free energy landscape calculated from the radius of gyration (R_g) and the root mean square deviation (RMSD) of the complex main chain (C_α atoms of HhpR and P atoms of DNA). Representative structures of HhpR–DNA complexes under different pressure conditions, with representative structures selected from the frames corresponding to the energy valley centers above. (**E**) The structure of HhpR dissociated from DNA at 0.1 MPa, which we define as the unbound state. (**F**) The structure of HhpR in contact with DNA at 0.1 MPa, which we define as the bound state. (**G**) Representative structure of the HhpR–DNA complex at 20 MPa, with the HhpR in close contact with the DNA and the Arm region close to the DNA major groove. (**H**) Representative structure of the HhpR–DNA complex at 52 MPa with the Arm region inserted into the DNA major groove.

of 6 and 5 Å (Figure 3G). Notably, at 52 MPa, the completely bound state becomes the dominant conformation (Figure 3D and H). Therefore, our computational results suggest that higher pressure indeed strengthens the interactions between HhpR and P_{hhp}.

Further structural inspections revealed more detailed conformational changes of both HhpR and DNA. Compared with low pressure, the DNA conformation at higher pressure is less bent, with average bending angles of 40°, 34° and 26° at 0.1, 20 and 52 MPa (Figure 4A), respectively. In other words, HhpR tends to stabilize the DNA conformation in a more extended form at higher pressure. As expected, the Arm region is highly flexible during the MD simulations and displays distinct conformational behaviors at different pressure conditions. At 0.1 MPa, as described earlier, an unbound conformation can be observed, resulting in fewer contacts between the Arm region and DNA. However, at higher pressure, the direct contacts between the Arm region and DNA are profoundly increased (Figure 4B). Particularly at 52 MPa, the Arm region can be inserted into the DNA major groove, which likely contributes to rigidify the DNA backbone (Figure 4C). Moreover, at high pressure, the HhpR binding increases the minor groove width of the specific binding site of HhpR, namely the TATA region at positions 13–16, exerted via one α-helix motif (residues 51–55, denoted as α2 hereafter). In particular, the minor groove widths at the 15 and 16 sites can be increased by ∼2 Å at 20 or 52 MPa compared with that at 0.1 MPa (Figure 4D). The widening of the minor groove width might be critical for initiating the gene transcription.

To pinpoint the specific recognition sites between HhpR and DNA at 52 MPa, we calculated the contact numbers for each HhpR residue with DNA. The contact heatmap shows that HhpR interacts with the specific sequence mainly via the N-terminus of the Arm region (residues 192–201) and one loop motif (residues 67–69) adjacent to the α2 region (Figure 4E and F). This finding is consistent with the above observations that the Arm region could penetrate into the DNA major groove and the α2 motif participates in widening the minor groove (Figure 4G). Notably, the HhpR residues K67 and R68 could establish stable salt-bridge interactions with the DNA backbone at the 14–17 sites, particularly at high pressure (Supplementary Figure S4A and B). Although D69 has no direct contact with DNA, it could transiently form salt bridges with R68 at low pressure (Supplementary Figure S4C and D). The above interaction network is likely responsible for guiding the α2 region moving toward the minor groove. Altogether, the CBS2 domain and the Arm region in HhpR are directly involved in the DNA recognition.

In vivo and *in vitro* mutagenic analyses of HhpR under high hydrostatic pressure

To further evaluate the functional roles of K67, R68 and D69, we designed a single mutant (D69A) and a triple mutant (K67A/R68A/D69A) of HhpR, and conducted *in vitro* binding assays with the wild-type (wt) P_{hhp} (labeled as P_{WT} in Figure 5A). The results show that compared with HhpR, both the single and the triple mutants could reduce the binding affinity of HhpR to P_{hhp} at 0.1 or 52 MPa (Figure 5A).

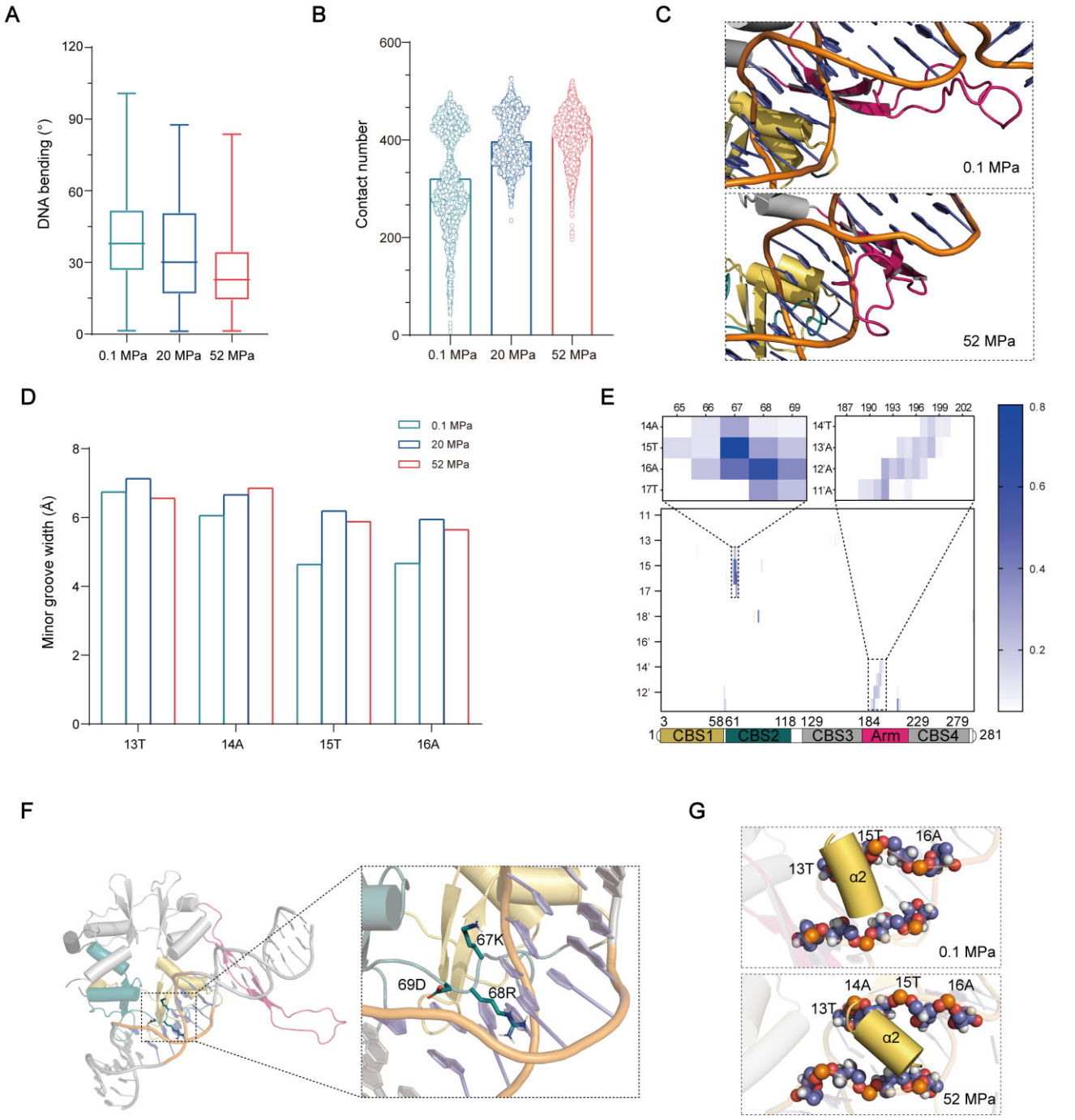

Figure 4. MD simulations of the protein HhpR and binding core region of P_{hhp} under hydrostatic pressures. (**A**) The total DNA bending angle at different hydrostatic pressures. (**B**) The average number of contacts between the Arm domain and DNA at different hydrostatic pressures. (**C**) Location of the Arm region in relation to the DNA major groove under different pressure conditions, with features selected from the representative structures above. (**D**) The width of the DNA minor groove (13–16 nt) bound to α2 under different hydrostatic pressures. The width of the minor groove was calculated using Curves+. (**E**) Heatmap of HhpR contact with the DNA core, with key contact areas shown enlarged above. (**F**) Position of sites 67–69 in the HhpR–DNA complex, highlighted using sticks. (**G**) Local features in sites 67–69 at 0.1 and 52 MPa, respectively, with features selected from the representative structures above.

Nevertheless, the binding affinity for both mutants is considerably stronger at 52 MPa than that at 0.1 MPa, which is consistent with the result for the wtHhpR. We further measured the binding between the triple mutant HhpR and the modified P_{hhp} with GC-riched UAS region (labeled as P_{CGmut}; see M3 in Figure 2A), and observed a significant reduced binding for P_{CGmut} relative to P_{hhp}, which, however, could be mitigated by applying increased HHP (Figure 5A).

Moreover, as suggested by MD simulations, the Arm region in HhpR might play a critical role in recognizing the target DNA, especially under HHP. To further verify this point, we replaced the Arm region with a short 'GSSG' linker

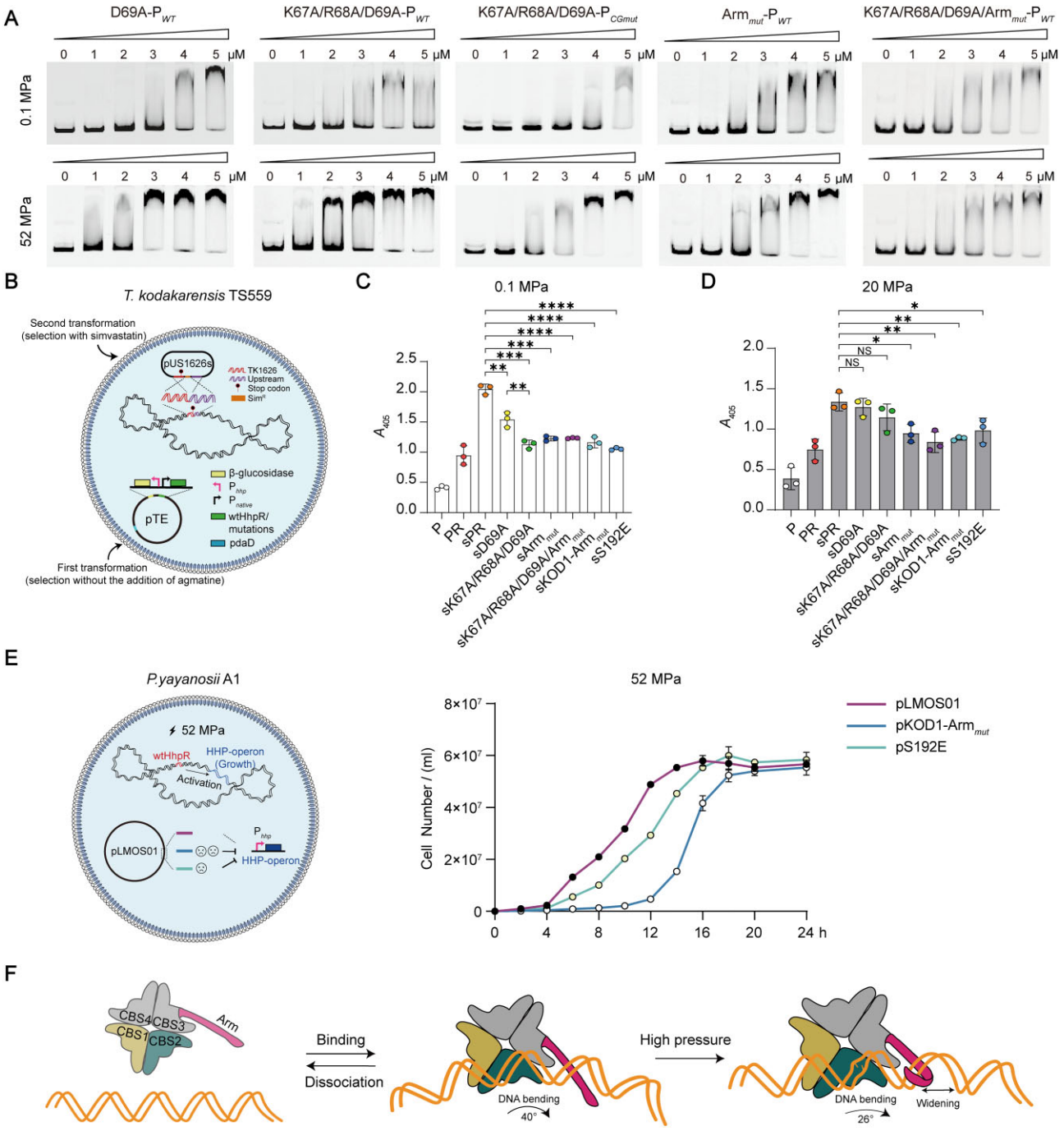

Figure 5. The mutational effects of the HhpR variants under HHP. (**A**) EMSAs showing binding of mutated HhpRs (following 52 MPa treatment or not) to probe P_{WT} or probe P_{CGmut} under 0.1 MPa. Protein concentrations in lanes 1–6 were 0, 1, 2, 3, 4 and 5 μM, respectively. P_{WT}, the wild-type promoter; P_{CGmut}, a mutant promoter P_{hhp} (GC-rich); Arm_{mut}, a mutant HhpR replaced the Arm region with a 'GSSG' linker. EMSAs were performed at 0.1 MPa. (**B**) Schematic diagram of the construction of *T. kodakarensis* TS559 recombinant strains. Pressurization reporter assay showing expression changes of different mutants under 0.1 MPa (**C**) and 20 MPa (**D**), respectively. P, *T. kodakarensis* TS559 with the β-glucosidase reporter gene controlled by P_{hhp}; PR, *T. kodakarensis* TS559 with the β-glucosidase reporter gene controlled by P_{hhp} and heterologous expression of HhpR controlled by native promoter; sPR, PR with *T. kodakarensis* TS559 homologous protein TK1626 whose reading frame was terminated at codon 3 by a nonsense mutation; sD69A, sPR with mutant D69A; sK67A/R68A/D69A, sPR with mutant K67A/R68A/D69A; $sArm_{mut}$, sPR with mutant HhpR-Arm_{mut}; sK67A/R68A/D69A/Arm_{mut}, sPR with mutant K67A/R68A/D69A and HhpR-Arm_{mut}; sKOD1-Arm_{mut}, sPR with mutant HhpR-Arm replaced of the same region of TK1626; sS192E, sPR with mutant S192E. The release of ONP was measured by the increase in A_{405}; the results shown above each strain designation are the averages (with error bars) of triplicate assays of lysates from three separate cultures of that strain. $^*P < 0.05$; $^{**}P < 0.01$; $^{***}P < 0.001$; $^{****}P < 0.0001$; NS, no significance. (**E**) Schematic diagram of the construction of *P. yayanosii* A1 recombinant strains and the effect of mutants (KOD1-Arm_{mut} and S192E) on the growth of *P. yayanosii* A1 under 52 MPa. (**F**) Model of HhpR-regulated transcriptional activation. The binding of HhpR to the UAS site results in a reduction in DNA bending and an increase in minor groove width under HHP, inducing transcriptional activation.

connecting CBS3 and CBS4 (see Arm$_{mut}$ in Figure 5A). The following EMSAs indicate that removal of the Arm region could significantly diminish the interaction between HhpR and P$_{hhp}$ (Figure 5A). Importantly, increasing pressure could impose an inconsiderable impact on the binding of Arm-deleted HhpR, highlighting the important role of the Arm region in the pressure-regulated property of HhpR. As expected, the combination of the triple K67A/R68A/D69A mutation with the Arm deletion could greatly weaken the promoter binding at 0.1 or 52 MPa (Figure 5A).

We further investigated the mutational effects of the above HhpR variants *in vivo*. As shown previously, the HHP-inducing promoter activity was not observed in *T. kodakarensis* (Figure 1C). Thus, we set out to introduce HhpR and the P$_{hhp}$-linked reporter system into *T. kodakarensis* (Figure 5B). Our results revealed that the P$_{hhp}$-linked reporter system exhibits a low level of glucosidase activity in the absence of HhpR (denoted as P in Figure 5C and D). However, expression of HhpR into the system could substantially increase the glucosidase activity (see PR in Figure 5C and D), suggesting that HhpR is indeed responsible for enhancing the gene expression via activating P$_{hhp}$. It is intriguing that the HhpR homologue protein in *T. kodakarensis*, TK1626, retains the binding with P$_{hhp}$ (Supplementary Figure S5), and abolishing the expression of TK1626 and overexpressing HhpR at the same time could further increase the promoter activity, indicating potential competitive P$_{hhp}$ binding for TK1626 and HhpR in *T. kodakarensis* (see sPR in Figure 5C and D).

Moreover, we examined how different HhpR mutants might affect the promoter activity in the absence of TK1626. Consistent with the above *in vitro* results, all four tested HhpR mutants could greatly impair the gene expression at low pressure (Figure 5C). Higher pressure could only rescue the regulatory functions of the HhpR variants with single (D69A) and triple (K67A/R68A/D69A) mutations but not for the Arm-deleted mutants (Figure 5D).

The Arm region is the decisive structural motif in HhpR regulating its pressure-induced property

To examine whether the lack of pressure-induced function of TK1626 stems from the difference of the Arm region between TK1626 and HhpR, we substituted the Arm region of HhpR with that of TK1626. Remarkably, this replacement is detrimental to the pressure-regulated function of HhpR (see sKOD1-Arm$_{mut}$ in Figure 5C and D), confirming that the Arm region indeed dictates the functional role of HhpR at higher pressure. Sequence alignment between TK1626 and HhpR reveals eight residue-mutation sites (Supplementary Figure S6A). Thus, to pinpoint the key residue(s) that are responsible for regulating the function of the Arm region, we performed MD simulations for TK1626 under different pressures.

Initial modeling of TK1626 showed that TK1626 has four CBS domains similar to HhpR and an Arm region connecting CBS3 and CBS4 (Supplementary Figure S6B). However, the MD results indicate that, in contrast to HhpR, the Arm region of TK1626 could not insert into the major groove and remains largely in the bulk region (Supplementary Figure S6D and E), resulting in an unbent DNA conformation. Further structural analyses show that, compared to HhpR, TK1626 lost most of its contact with DNA at the E192 site (Supplementary Figure S6C). This is likely due to the fact that E192 in TK1626 failed to form hydrogen bond with the DNA backbone, and its negatively charged side chain could also repulse the DNA chain (Supplementary Figure S6F). S192 in HhpR, however, could establish direct contact with DNA via forming hydrogen bond. To verify the above computational prediction, we introduced one S192E substitution in HhpR and tested the effects of this mutation via *in vivo* assays. The results show that the S192E mutation could profoundly impair the regulatory activity of HhpR at high pressure. Taken together, we conclude that the Arm region in HhpR plays a crucial role in the HHP-induced transcriptional activation, exerted mainly at the 192 position (Figure 5D).

To make it more reasonable, we further performed additional *in vivo* experiments in *P. yayanosii* to confirm the result. The gene cluster controlled by P$_{hhp}$ exhibits high expression at 52 MPa, which is the key operon regulating the growth of *P. yayanosii* under high pressure. As shown in Figure 5E, we used a new approach by utilizing the archaeal strong promoter (P2289, the promoter of gene TK2289 encoding archaeal histone B) to achieve overexpression of mutated HhpR (KOD1-Arm$_{mut}$ or S192E). In consequence, the overexpressed KOD1-Arm$_{mut}$ or S192E can competitively bind P$_{hhp}$ against the wtHhpR. Therefore, the crucial involvement of HhpR in activating transcription within specific region can be inferred from the growth under high pressure. Compared to *P. yayanosii*/pLMOS01, the growth rates of mutant recombinant strains (*P. yayanosii*/pKOD1-Arm$_{mut}$ and *P. yayanosii*/pS192E) were slower at 52 MPa. Notably, the exponential phase of the strain *P. yayanosii*/pKOD1-Arm$_{mut}$ (Figure 5E) was delayed ∼6 h. All results revealed that the Arm region plays an essential role in the pressure-regulated properties of HhpR (Figure 5F).

Analysis of homologous proteins of HhpR in the family Thermococcaceae

Homologous proteins of HhpR are widely distributed within the family Thermococcaceae (Supplementary Table S5). The phylogenetic analysis reveals a distinctive pattern wherein HhpR homologues from the genus *Pyrococcus* cluster together in a separated branch (Figure 6). Interestingly, when considering the sampling depths for the isolation of these Thermococcales members, a specific branch encompassing the HhpR homologue TK1626 from *T. kodakarensis* KOD1 is designated as a surface branch (highlighted in red in Figure 6). Notably, in this identified surface branch, homologous sequences of the HHP-responsive promoter P$_{hhp}$ observed in *P. yayanosii* are absent. We found that this distinct behavior between HhpR and TK1626 originated from their nonconserved Arm region, particularly at the 192 position, and the S192E substitution in HhpR could significantly decrease the transcription activity of HhpR. Intriguingly, the 192 site displays the highest sequence variance among all homologous HhpR proteins in the Thermococcaceae family (Supplementary Figure S8), necessitating future attempts to compare their HHP-induced activities. Nevertheless, TK1626 retains its ability to bind with P$_{hhp}$ (Supplementary Figure S5), indicating that TK1626-like CBS proteins are also potential transcriptional regulators,

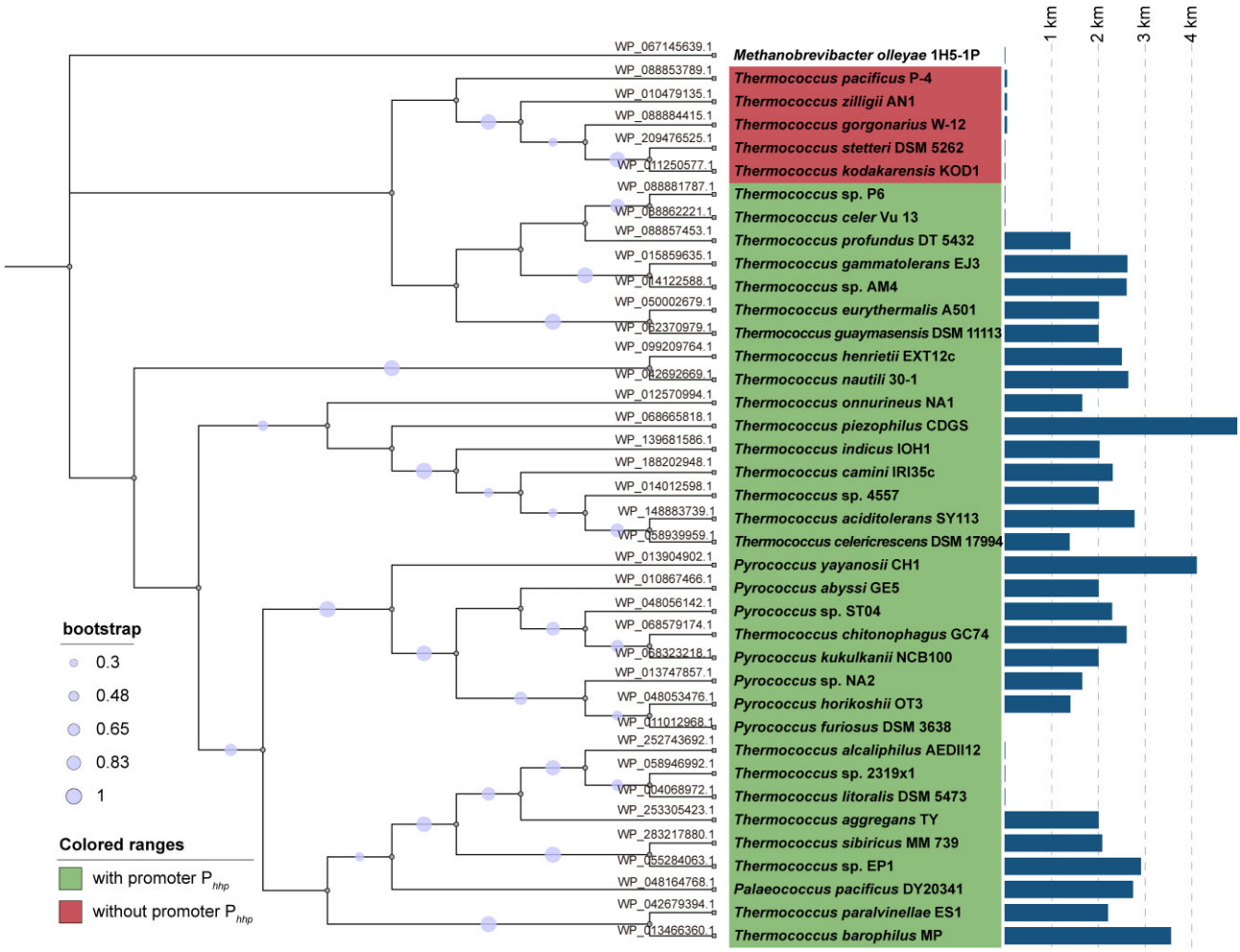

Figure 6. Phylogenetic analysis of HhpR proteins in Thermococcaceae. Phylogenetic trees were constructed using the neighbor-joining method, *Methanobrevibacter olleyae* 1H5-1P was used as an outgroup and bootstrap tests were used to assess branching confidence. Depth of species segregation was represented using cyan bar charts, and 39 species were further classified as present (low group) as well as absent (upper group) based on the presence of P_{hhp}-like promoters in the genome.

likely participating in transcriptional regulation under other conditions.

Discussion

The specific interaction between proteins and DNA is a fundamental aspect of biological sensing and the cellular response to environmental stresses (38). The CBS-containing proteins are notably prevalent in archaea (39). For example, in eight hyperthermophilic archaea strains of the family Thermococcaceae, the genome of each strain harbors 8–10 CBS-containing proteins (Supplementary Figure S7). Some of these CBS proteins also carry additional conservative domain with a discernible catalytic function, such as IMP dehydrogenase (WP_013906108.1, WP_011011399.1, WP_010868777.1, etc.). Combinations of CBS domains and HTH (helix–turn–helix)-type transcriptional regulator domain were also observed (WP_013904935.1, WP_011012935.1, WP_010867433.1, etc.). In contrast, some of the CBS-containing proteins are exclusively composed of the CBS domains (Supplementary Figure S7). Here, we found a transcriptional activator HhpR from *P. yayanosii* that contains four consecutive CBS domains and is highly sensitive to HHP. By combining computational simulations and experimental assays, we revealed the molecular mechanism underlying the DNA recognition by HhpR and the associated structural dynamic properties.

Notably, homologous sequence of neither the promoter P_{hhp} nor the downstream *hhpA* gene exists in *T. kodakarensis* KOD1. We showed that both of the homologous proteins HhpR (from *P. yayanosii*) and TK1626 (from *T. kodakarensis*) could bind to the P_{hhp}. Although TK1626 does not impose high-pressure-induced activation effect on the promoter P_{hhp}, the UAS motifs in the upstream region of four promoters (Supplementary Table S3) might be regulated by TK1626 in responding to other physiological signal or stress. This further supports that CBS-containing proteins are universal TFs in Thermococcales. Moreover, we aligned the promoter sequences of 39 homologous proteins of HhpR in Thermococcales. The core sequence features of typical archaeal promoters, i.e. BRE and TATA elements, were found but the UAS motif was not identified in the region upstream of BRE. The results showed that the CBS domains could not act as autoinhibitory regulatory units (Supplementary Figure S10).

TFs target their specific sites by specifically recognizing nucleobases (base readout) and/or DNA shapes (shape readout). Base readout normally occurs in DNA major or minor grooves. For example, TFs with HTH motifs primarily bind to the DNA major groove, thereby forming several specific hydrogen bonding interactions (40). Shape readout involves the recognition of the 3D DNA conformation rather than specific nucleobases; for example, TATA-binding protein (TBP) and the male sex determining factor SRY primarily interact with significantly deformed DNA (41). Moreover, asymmetrical shielding of DNA phosphates by positively charged residues and insertion of protein side chains into DNA bases could also trigger profound DNA bending. This significant DNA bending is mainly through interaction with the DNA minor groove at AT-rich sites (42). In comparison, for HhpR, at 0.1 MPa, its higher structural flexibility in solution (high entropy state) leads to a larger DNA bending angle (∼40°) due to the insertion of the α2 region into the minor groove. As pressure increases to 52 MPa, the system shifts toward a lower entropy state; therefore, the reaction becomes enthalpy-driven, reflected in the deeper insertion of the Arm region into the major groove, while the contribution of the α2 region to DNA binding decreases, as supported by our mutagenesis assays.

Archaea utilize a eukaryote-like transcription machinery to read the genetic information in the genomes organized in bacteria-like style. This transcription system encompasses RNAP subunits, basal transcription initiation factors (i.e. TBP, TFB and TFE) and elongation factors (including TFS, Spt4/5 and Elf1) (43). At present, our understanding of general transcription activation mechanisms in archaea largely revolves around the recruitment and stabilization of TBP or TFB at their respective promoter elements. Potent transcriptional activator 2 (Ptr2) was the first identified example of an archaeal transcriptional activator. Ptr2 was considered to interact directly with TBP to facilitate its recruitment to the TATA-box, thus functioning as a TBP recruitment factor (44). Similarly, TFB recruitment factor 1 activates transcription in *P. furiosus* via a mechanism that involves the stimulation of TFB recruitment to the promoter (45). More recently, the TFs EarA of *P. furiosus* and Tar of *T. kodakarensis* have been shown to exhibit transcriptional activation activity, via directly interacting with either TFB or TBP (15,46). Here, we identified a novel archaeal transcription activator, HhpR, which exerts its function under HHP. MD simulations revealed that the enhanced binding affinity of HhpR to the TA-rich UAS leads to a reduced DNA bending of the promoter P_{hhp}. In contrast, binding of TBP with promoter could cause severe bending of DNA backbones, as evidenced by the crystal structure (47). Furthermore, HhpR has been observed to bind to the TATA-box (Supplementary Figure S3B), indicating a potential competitive relationship with TBP. So, the interaction between HhpR and other TFs is worth to be further explored in the future.

Over the past decades, the effects of HHP on protein structure and function have been extensively studied using various biophysical techniques, including X-ray crystallography (48), nuclear magnetic resonance spectroscopy (49,50), infrared spectroscopy (51), calorimetry and MD simulations (49,52,53). These studies have established that high pressure could induce protein denaturation, unfolding and inactivation by imposing profound effects on the protein structures via, for example, modulating the compaction of protein structure (54), rearrangement of hydrogen bonding networks (48), distortion of secondary structures (54), disruption of hydrophobic interactions, salt-bridge interactions and increased vibrational frequencies (48,54–56), or influencing the dynamics of solvent waters (53,57,58). Our MD simulations observed that HHP could induce significant structural rearrangements of HhpR, particularly in the Arm region, which lead to profound structural compaction of HhpR, strengthened DNA binding and DNA deformation (Figure 5F).

In summary, our integrated biochemical and computational approaches provided new insights into the pressure adaptation mechanisms for a novel HHP-activated transcriptional regulator HhpR from the piezophilic archaeon *P. yayanosii*. To our knowledge, HhpR is the first reported CBS protein so far that serves as a transcriptional activator involved in the gene regulation responding to HHP. Our work significantly advanced the understanding of the pressure-regulated proteins and elucidated their structure–function relationships.

Data availability

The data underlying this article are available in the article and in its online supplementary material. Further data underlying this article will be shared on reasonable request to the corresponding author.

Supplementary data

Supplementary Data are available at NAR Online.

Acknowledgements

We thank Professor Xiang Xiao at the International Center for Deep Life Investigation, Shanghai Jiao Tong University, for support in research facilities and helpful discussions on the project.

Author contributions: C.L. and S.L. performed the molecular genetics experiments and the computational analyses and wrote the paper. Q.S. carried out preliminary data analysis. J.X. and L.D. designed the research and provided guidance on the project.

Funding

National Key Research and Development Program of China [2020YFA0906800]; National Natural Science Foundation of China [41976085, 42276091]; Natural Science Foundation of Shanghai Municipality [20ZR1425400, 21JC1403100]; Scientific and Technological Innovation Plan of Shanghai Science and Technology Committee [24Z510200306]; Shanghai Jiao Tong University [SL2022PT208]. Funding for open access charge: National Key Research and Development Program of China [2020YFA0906800].

Conflict of interest statement

None declared.

References

1. Sogin,M.L., Morrison,H.G., Huber,J.A., Welch,D.M., Huse,S.M., Neal,P.R., Arrieta,J.M. and Herndl,G.J. (2006) Microbial diversity in the deep sea and the underexplored "rare biosphere". *Proc. Natl Acad. Sci. U.S.A.*, **103**, 12115–12120.

2. Xiao,X., Zhang,Y. and Wang,F. (2021) Hydrostatic pressure is the universal key driver of microbial evolution in the deep ocean and beyond. *Environ. Microbiol. Rep.*, **13**, 68–72.
3. Oger,P.M. and Jebbar,M. (2010) The many ways of coping with pressure. *Res. Microbiol.*, **161**, 799–809.
4. Jebbar,M., Franzetti,B., Girard,E. and Oger,P. (2015) Microbial diversity and adaptation to high hydrostatic pressure in deep-sea hydrothermal vents prokaryotes. *Extremophiles*, **19**, 721–740.
5. Abe,F. (2007) Exploration of the effects of high hydrostatic pressure on microbial growth, physiology and survival: perspectives from piezophysiology. *Biosci. Biotechnol. Biochem.*, **71**, 2347–2357.
6. Zhang,Y., Li,X., Bartlett,D.H. and Xiao,X. (2015) Current developments in marine microbiology: high-pressure biotechnology and the genetic engineering of piezophiles. *Curr. Opin. Biotechnol.*, **33**, 157–164.
7. Vannier,P., Michoud,G., Oger,P., Marteinsson,V. and Jebbar,M. (2015) Genome expression of *Thermococcus barophilus* and *Thermococcus kodakarensis* in response to different hydrostatic pressure conditions. *Res. Microbiol.*, **166**, 717–725.
8. Michoud,G. and Jebbar,M. (2016) High hydrostatic pressure adaptive strategies in an obligate piezophile *Pyrococcus yayanosii*. *Sci. Rep.*, **6**, 27289.
9. Xu,J., Liu,L., Xu,M., Oger,P., Wang,F., Jebbar,M. and Xiao,X. (2011) Complete genome sequence of the obligate piezophilic hyperthermophilic archaeon *Pyrococcus yayanosii* CH1. *J. Bacteriol.*, **193**, 4297–4298.
10. Zeng,X., Birrien,J.L., Fouquet,Y., Cherkashov,G., Jebbar,M., Querellou,J., Oger,P., Cambon-Bonavita,M.A., Xiao,X. and Prieur,D. (2009) *Pyrococcus* CH1, an obligate piezophilic hyperthermophile: extending the upper pressure-temperature limits for life. *ISME J.*, **3**, 873–876.
11. Lipscomb,G.L., Keese,A.M., Cowart,D.M., Schut,G.J., Thomm,M., Adams,M.W.W. and Scott,R.A. (2009) SurR: a transcriptional activator and repressor controlling hydrogen and elemental sulphur metabolism in *Pyrococcus furiosus*. *Mol. Microbiol.*, **71**, 332–349.
12. Vierke,G., Engelmann,A., Hebbeln,C. and Thomm,M. (2003) A novel archaeal transcriptional regulator of heat shock response. *J. Biol. Chem.*, **278**, 18–26.
13. Lee,S.J., Moulakakis,C., Koning,S.M., Hausner,W., Thomm,M. and Boos,W. (2005) TrmB, a sugar sensing regulator of ABC transporter genes in *Pyrococcus furiosus* exhibits dual promoter specificity and is controlled by different inducers. *Mol. Microbiol.*, **57**, 1797–1807.
14. Reichelt,R., Ruperti,K.M.A., Kreuzer,M., Dexl,S., Thomm,M. and Hausner,W. (2018) The transcriptional regulator TFB-RF1 activates transcription of a putative ABC transporter in *Pyrococcus furiosus*. *Front. Microbiol.*, **9**, 838.
15. Yamamoto,Y., Kanai,T., Kaneseki,T. and Atomia,H. (2019) The TK0271 protein activates transcription of aromatic amino acid biosynthesis genes in the hyperthermophilic archaeon *Thermococcus kodakarensis*. *mBio*, **10**, e01213-19.
16. Alex,B. (1997) The structure of a domain common to archaebacteria and the homocystinuria disease protein. *Trends Biochem. Sci.*, **22**, 12–13.
17. Baykov,A.A., Tuominen,H.K. and Lahti,R. (2011) The CBS domain: a protein module with an emerging prominent role in regulation. *ACS Chem. Biol.*, **6**, 1156–1163.
18. Pimkin,M., Pimkina,J. and Markham,G.D. (2009) A regulatory role of the Bateman domain of IMP dehydrogenase in adenylate nucleotide biosynthesis. *J. Biol. Chem.*, **284**, 7960–7969.
19. McLean,J.E., Hamaguchi,N., Belenky,P., Mortimer,S.E., Stanton,M. and Hedstrom,L. (2004) Inosine 5′-monophosphate dehydrogenase binds nucleic acids *in vitro* and *in vivo*. *Biochem. J.*, **379**, 243–251.
20. Aguado-Llera,D., Oyenarte,I., Martinez-Cruz,L.A. and Neira,J.L. (2010) The CBS domain protein MJ0729 of *Methanocaldococcus jannaschii* binds DNA. *FEBS Lett.*, **584**, 4485–4489.
21. Ragunathan,P., Kumarevel,T., Agari,Y., Shinkai,A., Kuramitsu,S., Yokoyama,S. and Ponnuraj,K. (2008) Crystal structure of ST2348, a CBS domain protein, from hyperthermophilic archaeon *Sulfolobus tokodaii*. *Biochem. Biophys. Res. Commun.*, **375**, 124–128.
22. Gómez-García,I., Oyenarte,I. and Martínez-Cruz,L.A. (2010) The crystal structure of protein MJ1225 from *Methanocaldococcus jannaschii* shows strong conservation of key structural features seen in the eukaryal γ-AMPK. *J. Mol. Biol.*, **399**, 53–70.
23. Li,X., Fu,L., Li,Z., Ma,X., Xiao,X. and Xu,J. (2015) Genetic tools for the piezophilic hyperthermophilic archaeon *Pyrococcus yayanosii*. *Extremophiles*, **19**, 59–67.
24. Gehring,A.M., Sanders,T.J. and Santangelo,T.J. (2017) Markerless gene editing in the hyperthermophilic archaeon *Thermococcus kodakarensis*. *Bio Protoc.*, **7**, e2604.
25. Song,Q., Li,Z., Chen,R., Ma,X., Xiao,X. and Xu,J. (2019) Induction of a toxin–antitoxin gene cassette under high hydrostatic pressure enables markerless gene disruption in the hyperthermophilic archaeon *Pyrococcus yayanosii*. *Appl. Environ. Microbiol.*, **85**, e02662.
26. Santangelo,T.J., Cubonova,L., Matsumi,R., Atomi,H., Imanaka,T. and Reeve,J.N. (2008) Polarity in archaeal operon transcription in *Thermococcus kodakaraensis*. *J. Bacteriol.*, **190**, 2244–2248.
27. Li,Z., Song,Q., Wang,Y., Xiao,X. and Xu,J. (2018) Identification of a functional toxin–antitoxin system located in the genomic island PYG1 of piezophilic hyperthermophilic archaeon *Pyrococcus yayanosii*. *Extremophiles*, **22**, 347–357.
28. Jumper,J., Evans,R., Pritzel,A., Green,T., Figurnov,M., Ronneberger,O., Tunyasuvunakool,K., Bates,R., Žídek,A., Potapenko,A., *et al.* (2021) Highly accurate protein structure prediction with AlphaFold. *Nature*, **596**, 583–589.
29. Li,S., Olson,W.K. and Lu,X.J. (2019) Web 3DNA 2.0 for the analysis, visualization, and modeling of 3D nucleic acid structures. *Nucleic Acids Res.*, **47**, W26–W34.
30. Yan,Y., Zhang,D., Zhou,P., Li,B. and Huang,S.-Y. (2017) HDOCK: a web server for protein–protein and protein–DNA/RNA docking based on a hybrid strategy. *Nucleic Acids Res.*, **45**, W365–W373.
31. Abraham,M.J., Murtola,T., Schulz,R., Páll,S., Smith,J.C., Hess,B. and Lindahl,E. (2015) GROMACS: high performance molecular simulations through multi-level parallelism from laptops to supercomputers. *SoftwareX*, **1-2**, 19–25.
32. Abascal,J.L. and Vega,C. (2005) A general purpose model for the condensed phases of water: TIP4P/2005. *J. Chem. Phys.*, **123**, 234505.
33. Hölzl,C. and Horinek,D. (2018) Pressure increases the ice-like order of water at hydrophobic interfaces. *Phys. Chem. Chem. Phys.*, **20**, 21257–21261.
34. Maier,J.A., Martinez,C., Kasavajhala,K., Wickstrom,L., Hauser,K.E. and Simmerling,C. (2015) ff14SB: improving the accuracy of protein side chain and backbone parameters from ff99sb. *J. Chem. Theory Comput.*, **11**, 3696–3713.
35. Ivani,I., Dans,P.D., Noy,A., Pérez,A., Faustino,I., Hospital,A., Walther,J., Andrio,P., Goñi,R., Balaceanu,A., *et al.* (2015) Parmbsc1: a refined force field for DNA simulations. *Nat. Methods*, **13**, 55–58.
36. Fine,R.A. and Millero,F.J. (1973) Compressibility of water as a function of temperature and pressure. *J. Chem. Phys.*, **59**, 5529–5536.
37. Lavery,R., Moakher,M., Maddocks,J.H., Petkeviciute,D. and Zakrzewska,K. (2009) Conformational analysis of nucleic acids revisited: Curves+. *Nucleic Acids Res.*, **37**, 5917–5929.
38. Rohs,R., Jin,X., West,S.M., Joshi,R., Honig,B. and Mann,R.S. (2010) Origins of specificity in protein–DNA recognition. *Annu. Rev. Biochem.*, **79**, 233–269.
39. Martínez-Cruz,L.A., Encinar,J.A., Kortazar,D., Prieto,J., Gómez,J., Fernández-Millán,P., Lucas,M., Arribas,E.A., Fernández,J.A., Martínez-Chantar,M.L., *et al.* (2009) The CBS domain protein MJ0729 of *Methanocaldococcus jannaschii* is a thermostable

protein with a pH-dependent self-oligomerization. *Biochemistry*, **48**, 2760–2776.
40. Luscombe,N.M., Austin,S.E., Berman,H.M. and Thornton,J.M. (2000) An overview of the structures of protein–DNA complexes. *Genome Biol.*, **1**, reviews001.
41. Bewley,C.A., Gronenborn,A.M. and Clore,G.M. (1998) Minor groove-binding architectural proteins structure, function, and DNA recognition. *Annu. Rev. Biophys. Biomol. Struct.*, **27**, 105–131.
42. Privalov,P.L., Dragan,A.I. and Crane-Robinson,C. (2009) The cost of DNA bending. *Trends Biochem. Sci.*, **34**, 464–470.
43. Wenck,B. and Santangelo,T. (2020) Archaeal transcription. *Transcription*, **11**, 199–210.
44. Ouhammouch,M., Langham,G.E., Hausner,W., Simpson,A.J., EI-Sayed,N.M.A. and Geiduschek,E.P. (2005) Promoter architecture and response to a positive regulator of archaeal transcription. *Mol. Microbiol.*, **56**, 625–637.
45. Ochs,S.M., Thumann,S., Richau,R., Weirauch,M.T., Lowe,T.M., Thomm,M. and Hausner,W. (2012) Activation of archaeal transcription mediated by recruitment of transcription factor B. *J. Biol. Chem.*, **287**, 18863–18871.
46. Stöckl,R., Nißl,L., Reichelt,R., Rachel,R., Grohmann,D. and Grünberger,F. (2023) The transcriptional regulator EarA and intergenic terminator sequences modulate archaellation in *Pyrococcus furiosus*. *Front. Microbiol.*, **14**, 1241399.
47. Kim,J.L., Nikolov,D.B. and Burley,S.K. (1993) Co-crystal structure of TBP recognizing the minor groove of a TATA element. *Nature*, **365**, 520–527.
48. Nagae,T., Yamada,H. and Watanabe,N. (2018) High-pressure protein crystal structure analysis of *Escherichia coli* dihydrofolate reductase complexed with folate and $NADP^+$. *Acta Crystallogr. D*, **74**, 895–905.
49. Roche,J., Caro,J.A., Norberto,D.R., Barthe,P., Roumestand,C., Schlessman,J.L., Garcia,A.E., García-Moreno,E.B. and Royer,C.A. (2012) Cavities determine the pressure unfolding of proteins. *Proc. Natl Acad. Sci. U.S.A.*, **109**, 6945–6950.
50. Day,R. and García,A.E. (2007) Water penetration in the low and high pressure native states of ubiquitin. *Proteins*, **70**, 1175–1184.
51. Panick,G., Malessa,R., Winter,R., Rapp,G., Frye,K.J. and Royer,C.A. (1998) Structural characterization of the pressure-denatured state and unfolding/refolding kinetics of staphylococcal nuclease by synchrotron small-angle X-ray scattering and Fourier-transform infrared spectroscopy. *J. Mol. Biol.*, **275**, 389–402.
52. Roccatano,D., Wakai,N., Takemura,K., Morita,T. and Kitao,A. (2014) Mechanism of deep-sea fish α-actin pressure tolerance investigated by molecular dynamics simulations. *PLoS One*, **9**, e85852.
53. Collins,M.D., Hummer,G., Quillin,M.L., Matthews,B.W. and Gruner,S.M. (2005) Cooperative water filling of a nonpolar protein cavity observed by high-pressure crystallography and simulation. *Proc. Natl Acad. Sci. U.S.A.*, **102**, 16668–16671.
54. Heremans,K. and Smeller,L. (1998) Protein structure and dynamics at high pressure. *Biochim. Biophys. Acta*, **1386**, 353–370.
55. Calandrini,V., Hamon,V., Hinsen,K., Calligari,P., Bellissent-Funel,M.C. and Kneller,G.R. (2008) Relaxation dynamics of lysozyme in solution under pressure: combining molecular dynamics simulations and quasielastic neutron scattering. *Chem. Phys.*, **345**, 289–297.
56. Teixeira,S.C.M., Penhallurick,R., Hoopes,J.T., Hemley,R.J. and Ichiye,T. (2019) High-pressure structural studies of dihydrofolate reductase in solution. *Biophys. J.*, **116**, 336a.
57. Sarupria,S., Ghosh,T., García,A.E. and Garde,S. (2010) Studying pressure denaturation of a protein by molecular dynamics simulations. *Proteins*, **78**, 1641–1651.
58. Chalikian,T.V. and Macgregor,R.B. (2009) Origins of pressure-induced protein transitions. *J. Mol. Biol.*, **394**, 834–842.

Received: June 20, 2024. **Revised:** December 13, 2024. **Editorial Decision:** December 16, 2024. **Accepted:** December 24, 2024